

OVERLAPPING MULTI-DOMAIN SPECTRAL METHOD FOR NON-DARCIAN MIXED CONVECTION CHEMICALLY REACTING FLOW OF MICROPOLAR FLUID OVER A FLAT PLATE IN A POROUS MEDIA

Musawenkhosi Patson Mkhathshwa^{1,†}, Sandile Sydney Motsa^{1,2},
Mekonnen Shiferaw Ayano² and Precious Sibanda¹

Abstract An efficient overlapping multi-domain spectral method is presented and used in the analysis of a two-dimensional steady laminar MHD mixed convection flow, heat and mass transfer over a vertical flat plate embedded in a porous medium. The effect of chemical reaction, thermal radiation, heat source/sink and other parameters influencing the flow has been analyzed by imposing magnetic force transverse to the plate in a non-Darcy porous medium with constant wall temperature and concentration conditions. The flow equations are expressed in dimensionless form and solved using overlapping multi-domain bivariate spectral local linearization method (OMD-BSLLM). An analysis of the convergence and accuracy of the OMD-BSLLM is given using error norms and residual errors. Comparisons with previously published work for special cases of the problem are performed and excellent concurrence is found; hence reliable results are being presented. The influence of certain parameters on the fluid properties and flow characteristics is analyzed. The skin friction, heat and mass transfer coefficients are presented for the concentrated flow and the turbulent boundary layer flow. The flow characteristics are found to be smaller for turbulent boundary layer flows than concentrated particle flows. This type of flow has an application in catalytic and chromatographic reactions, packed absorption and distillation towers.

Keywords Spectral local linearisation method, overlapping multi-domain grid, micropolar fluid, thermal radiation, chemical reaction, heat source/sink.

MSC(2010) 76A05, 76R99, 76M22, 76M60.

1. Introduction

Extensive studies have been carried out on combined heat and mass transfer in between flows under the assumption of different physical real-life situation. Flows through the porous medium are quite prevalent in nature and the study of such flows has applications in environmental and engineering fields such as in enhanced

[†]The corresponding author. Email address:patsonmkhatshwa@gmail.com (M. Mkhathshwa)

¹School of Mathematics, Statistics & Computer Science, University of Kwazulu Natal, Private Bag X01, Scottsville, 3209, Pietermaritzburg, South Africa

²Department of Mathematics, University of Eswatini, Kingdom of Eswatini

oil recovery, paper and textile coating, and composite manufacturing processes. Early studies on porous media used Darcy's law which is a linear empirical relation between the velocity and the pressure drop across the porous medium. In many practical applications, for example, packed sphere beds, the porous medium is bounded by an impermeable wall, has higher flow rates, and nonhomogeneous porosity variation near the wall, making Darcy's law inapplicable [8]. The non-Darcian convective heat transport in porous media has been a subject of interest to many researchers. Subsequently, the Darcian law has been modified to include the effects of inertia. Inertial effects on porous media transport have been generally studied using the Darcy-Forchheimer model which uses a quadratic impedance term for inertial drag. Chien and Cha'o [8] reported that the inclusion of non-Darcian effects significantly alters the flow and heat transfer characteristics from those predicted by the traditional Darcy's model. Ranganathan and Viskanta [28] studied mixed convection boundary layer flow along a vertical porous medium, and their results show that the inertial and viscous effects have a significant influence on the flow. Giving specific attention to flow through a porous medium in the vicinity of an impermeable boundary, Vafai and Tien [35] examined the effects of a solid boundary and the inertial forces on flow and heat transfer in porous media.

The studies on magnetohydrodynamics (MHD) flow for electrically conducting fluid past a vertical surface are important from a technological point of view. These studies have a bearing on industrial applications such as power generators, turbomachinery, solidification process in metallurgy and some astrophysical problems. In most cases, the Hall term is ignored in applying Ohms law as it has no marked effect for small magnetic fields. However, to study the effects of strong magnetic fields on the electrically conducting fluid flow, the influence of the electromagnetic force is noticeable. The effects of Hall current on MHD free or convective flow along a vertical surface with or without mass transfer have been studied by several authors [3, 18, 19, 27, 29]. When convective flows occur at high temperatures, radiation effects on the flow become significant. Many processes in engineering areas occur at high temperatures and knowledge of radiative heat transfer becomes very important for the design of pertinent equipment. The effect of radiation has been examined by several researchers including Hossain and Takhar [20], Muthucumaraswamy and Kumar [26], and Kinyanjui et al. [21] to name a few. Various practical diffusive operations include the molecular diffusion of a species with chemical reaction within or at the boundary. Chemical reaction can be classified as either homogeneous or heterogeneous reaction. Homogeneous reaction take place uniformly throughout a given phase. The species generation in a homogeneous chemical reaction is similar to internal source of heat generation. On the other hand, heterogeneous chemical reaction occurs in a restricted region or within the boundary of a phase. For that reason, it can be taken as a boundary condition analogous to the heat flux condition in heat transfer. The study of heat and mass transfer analysis in the presence of chemical reaction is important due to its existence in numerous fields of science and engineering. Rashad and EL-Kabeir [32] investigated coupled heat and mass transfer in transient flow by mixed convection over a vertical stretched sheet embedded in a fluid-saturated porous medium with chemical reaction. Chamkha et al. [11] analyzed the effects of thermal radiation and chemical reaction on heat and mass transfer by non-Darcian free convection past a vertical cylinder embedded in a porous medium.

Micropolar convection flows have been analyzed by many researchers following

the seminal work of Eringen [13], who introduced the micropolar fluid. The theory of fluids with microstructures has been the subject of interest to a large number of investigations. These investigations are realistic and important from a technological point of view. The classical theories of continuum mechanics are inadequate to explain the microscopic manifestations of complex hydrodynamic behaviour. Microcontinuum theory or generalized continuum theories incorporate independent deformations of the microstructure inside of a material point. There are a number of microcontinuum theories, namely couple stress, micropolar, microstretch and micromorphic [14, 15]. These theories impose more or less constraints on the motion of microstructure inside of a material point. In microstretch theory, it is assumed that the microstructure of each material point can undergo expansion or contraction independently in addition to translation and rigid rotation. This theory is a generalization of micropolar theory, in which the microstructure can only have translation and rigid rotation. Micromorphic theory constitutes extensions of the classical field theories concerned with the deformations, motions, and electromagnetic interactions of material media, as continua, in microscopic time and space scales. In micromorphic theory, a material body is considered as a continuous collection of deformable particles, each with finite size and inner structure. A subclass of these fluids introduced by Eringen [16], is the micropolar fluids, which exhibit microrotational effects observed in colloidal solutions, blood, dielectric fluids, plasmas, liquid crystals, etc. The theory and applications of micropolar fluids is explained in the monographs by Ariman et al. [5, 6] and in Lukaszewicz [22]. Such fluids find applications in the purification of crude oil, in polymer technologies, centrifugal separation processes, cooling tower dynamics, chemical reaction engineering, metallurgical drawing of filaments and solar energy systems.

Many researchers have examined different flow geometries for micropolar fluid. Modather et al. [23] studied the impact of chemical reaction on heat and mass transfer of micropolar fluids in a saturated porous medium over an infinite moving plate with transverse magnetic field. Ayano [1] analyzed MHD mixed convection flow of micropolar fluid over a semi-infinite plate with uniform heat and mass flux in the presence of Hall and Ion-slip currents. Chamkha et al. [9] investigated the influence of radiation and chemical reaction on coupled heat and mass transfer by MHD natural convection flow of a micropolar fluid over a permeable truncated cone. Srinivasacharya and Mendu [33] examined MHD free convection heat and mass transfer in a micropolar fluid over a vertical plate with radiation and chemical reaction effect. The influence of heat source/sink on MHD flow of micropolar fluid along a shrinking sheet was investigated by Ahmad [4]. Rashad et al. [30] studied the effects of chemical reaction and thermal radiation on coupled heat and mass transfer by a natural convection flow of a micropolar fluid over a vertical flat plate embedded in a porous medium. Rashad et al. [31] considered coupled heat and mass transfer by mixed convection flow of a micropolar fluid past a continuously moving isothermal vertical surface saturated in a thermally and solutally stratified medium with chemical reaction. Chamkha [12] considered the problem of unsteady heat and mass transfer by mixed convection flow of a micropolar fluid near the region of the stagnation point on a double-infinite vertical flat plate in the presence of chemical reaction and thermal radiation. Ayano and Mathunjwa [2] investigated the effects of chemical reaction and radiation on MHD flow of micropolar fluid over vertical plate with varying temperature. Mishra et al. [24] studied the flow of micropolar fluid along with heat and mass transfer over a porous shrinking sheet in the presence of

heat source and chemical reaction.

The objective of this study is to investigate the effects of simultaneous heat and mass transfer on the mixed convection MHD flow of an incompressible electrically conducting micropolar fluid over an infinite vertical plate embedded in a saturated porous medium by taking into account the effects of radiation, heat source/sink, Hall current and chemical reaction. To the best of the authors' knowledge, the present problem has not been studied. The transformed nonlinear partial differential equations (PDEs) are solved by an efficient overlapping multi-domain bivariate spectral local linearisation method. The novelty of the present work is the use of an improved multi-domain spectral collocation-based method to find the solution to the problem. The need to continually improve on existing spectral collocation-based methods for solving nonlinear differential equations that cannot be solved analytically cannot be overstated. Since the previous multi-domain approach has been applied to either space or time but not both in existing spectral collocation-based methods, the present work incorporates the multi-domain technique in both space and time intervals to increase the accuracy of the method. In addition to that, the method uses the overlapping grid strategy when splitting the space interval. The overlapping grid approach holds a great potential of improving accuracy of the method since it produces less dense (sparse) matrices that can be inverted in a computationally efficient manner. The sparsity of matrices due to overlapping sub-domains minimizes the storage of large matrices and make it easy to perform matrix-vector multiplications. Consequently, the proposed method will require less computer memory and computational time to produce highly accurate results. In the present study, we describe the development of the method and demonstrate its applicability to a system of nonlinear boundary layer equations. We also highlight the accuracy, robustness and efficiency of the method when applied to highly nonlinear PDEs with significant complexities. To establish the accuracy of the numerical method, certain limiting solutions of the momentum and energy equations are considered. Since the method combines the bivariate spectral local linearisation method [25], non-overlapping and overlapping multi-domain technique, for reference purposes we shall refer to the method as overlapping multi-domain bivariate spectral local linearisation method (OMD-BsLLM).

2. Mathematical formulation of the problem

We consider the mixed convection boundary-layer flow in the vicinity of an impermeable vertical plate embedded in a porous medium which is saturated with micropolar fluid. The fluid is assumed laminar, incompressible, two-dimensional and, the ambient temperature and concentration are considered as T_∞ and C_∞ , respectively. The x -coordinate is along the plate, the y -coordinate is measured normal to the plate. The vertical plate chosen in this work is infinitely long, concentration, temperature and velocity equations are only depend on y . A uniform magnetic field is applied normal to the plate and the induced magnetic field is negligible in comparison with the applied one suggesting a small magnetic Reynolds number. The effect of Hall current is taken into account. It is assumed that there is no applied voltage of which implies the absence of an electric field. All fluid properties are considered to be constant except for the density variation which induces the buoyancy force. With these assumptions and taking into account the Boussinesq and boundary layer approximations the basic equations of a micropolar fluid in a

Darcy-Forchheimer saturated porous medium can be written as:

$$\frac{\partial u}{\partial x} + \frac{\partial v}{\partial y} = 0 \quad (2.1)$$

$$\begin{aligned} \frac{1}{\epsilon^2} \left(u \frac{\partial u}{\partial x} + v \frac{\partial u}{\partial y} \right) &= \frac{1}{\epsilon} \frac{\mu + \kappa}{\rho} \frac{\partial^2 u}{\partial y^2} + \frac{\kappa}{\rho} \frac{\partial \Gamma}{\partial y} + g^* [\beta_T (T - T_\infty) + \beta_c (C - C_\infty)] \\ &\quad - \frac{\nu}{K_p} u - \frac{b}{K_p} u^2 - \frac{1}{\epsilon} \frac{\sigma B_0^2}{\rho(1 + \beta_h^2)} (u + \beta_h w) \end{aligned} \quad (2.2)$$

$$\frac{1}{\epsilon^2} \left(u \frac{\partial w}{\partial x} + v \frac{\partial w}{\partial y} \right) = \frac{1}{\epsilon} \frac{\mu + \kappa}{\rho} \frac{\partial^2 w}{\partial y^2} - \frac{\nu}{K_p} w - \frac{b}{K_p} w^2 + \frac{1}{\epsilon} \frac{\sigma B_0^2}{\rho(1 + \beta_h^2)} (\beta_h u - w) \quad (2.3)$$

$$\frac{1}{\epsilon} \rho j \left(u \frac{\partial \Gamma}{\partial x} + v \frac{\partial \Gamma}{\partial y} \right) = \gamma \frac{\partial^2 \Gamma}{\partial y^2} - 2\kappa \Gamma - \kappa \frac{\partial u}{\partial y} \quad (2.4)$$

$$u \frac{\partial T}{\partial x} + v \frac{\partial T}{\partial y} = \frac{\lambda}{\rho C_p} \frac{\partial^2 T}{\partial y^2} - \frac{Q_0}{\rho C_p} (T - T_\infty) - \frac{1}{\rho C_p} \frac{\partial q_r}{\partial y} \quad (2.5)$$

$$u \frac{\partial C}{\partial x} + v \frac{\partial C}{\partial y} = D \frac{\partial^2 C}{\partial y^2} - K_1 (C - C_\infty) \quad (2.6)$$

where u and v are velocity components in the x and y directions, Γ is microrotation, j is the micro-inertia density, ρ is the fluid density, μ , κ and γ are the material constants (viscosity coefficients), g^* is the acceleration due to gravity, β_T is the coefficient of thermal expansion, β_c is the coefficient of solutal expansion, B_0 magnetic field intensity, $\beta_h = \sigma \beta B_0$ is Hall parameter, α is the thermal diffusivity, C_p is the specific heat, K_p is the permeability of the porous medium, D is the mass diffusivity, λ is the thermal conductivity and K_1 is the chemical reaction parameter. The term $Q(T_w - T_\infty)$ is the heat generated or absorbed per unit volume, where Q is a constant, which may be either positive ($T_w < T_\infty$) for a heat sink or negative ($T_w > T_\infty$) for a heat source. The radiative heat flux term by using the Rosseland approximation is given by $q_r = -4 \frac{\sigma}{3\chi} \frac{\partial T^4}{\partial y}$. We assume that the temperature differences within the flow are sufficiently small such that T^4 may be expressed as a linear function of the temperature

$$T^4 \cong 4T_\infty^3 T - T_\infty^4.$$

The boundary conditions for a stationary plate with constant heat flux from the plate to the fluid are given by

$$u = v = w = 0, \quad \Gamma = -n \frac{\partial u}{\partial y}, \quad T = T_w, \quad C = C_w, \text{ at } y = 0 \quad (2.7)$$

$$u = U_\infty, \quad w = 0, \quad \Gamma = 0, \quad T = T_\infty, \quad C = C_\infty, \text{ as } y \rightarrow \infty, \quad (2.8)$$

where n ($0 \leq n \leq 1$) is the constant that is related to micro-gyration vector and shear stress. The case $n = 0$ represents concentrated particle flows in which the microelements close to the wall surface are unable to rotate. This case is also known as the strong concentration of microelements. The case $n = 0.5$ indicates the vanishing of anti-symmetric part of stress tensor and denotes the weak concentration of microelements. The case $n = 1$ is used for modelling turbulent boundary layer flows. In the present study we shall consider $n = 0$ and $n = 1$.

To transform the nonlinear PDEs (2.1)-(2.6) into dimensionless form, we introduce the following transformations

$$\Psi = (\nu U_\infty x)^{1/2} f(\xi, \eta), \quad \xi = \frac{x}{L}, \quad \eta = y \left(\frac{U_\infty}{\nu x} \right)^{1/2}, \quad w = U_\infty g(\xi, \eta), \quad (2.9)$$

$$\Gamma = U_\infty \left(\frac{U_\infty}{\nu x} \right)^{1/2} \omega(\xi, \eta), \quad \theta(\xi, \eta) = \frac{T - T_\infty}{T_w - T_\infty}, \quad \phi(\xi, \eta) = \frac{C - C_\infty}{C_w - C_\infty}, \quad (2.10)$$

where Ψ is the stream function with $u = \frac{\partial \Psi}{\partial y}$ and $v = -\frac{\partial \Psi}{\partial x}$, thus satisfying the mass conservation equation. Substituting equation (2.9) - (2.10) into equations (2.1) - (2.6), we obtain the following non-dimensional equations

$$\begin{aligned} \frac{1}{\epsilon(1-N)} f''' + \frac{3}{4\epsilon^2} f f'' - \frac{1}{2\epsilon^2} f'^2 + \left(\frac{N}{1-N} \right) \omega' + \theta + \lambda \phi - \frac{\xi^{1/2}}{D_a Re_L^{1/2}} f' \\ - \xi^{1/2} \frac{Ha^2}{\epsilon(1+\beta_h^2) Re_L^{1/2}} (f' + \beta_h g) - \xi \frac{F_s}{D_a} f'^2 = \frac{\xi}{\epsilon^2} \left(f' \frac{\partial f'}{\partial \xi} - f'' \frac{\partial f}{\partial \xi} \right), \end{aligned} \quad (2.11)$$

$$\begin{aligned} \frac{1}{\epsilon(1-N)} g'' + \frac{3}{4\epsilon^2} f g' - \frac{1}{2\epsilon^2} g f' - \xi^{1/2} \frac{1}{D_a Re_L^{1/2}} g - \xi \frac{F_s}{D_a} g^2 \\ + \xi^{1/2} \frac{Ha^2}{\epsilon(1+\beta_h^2) Re_L^{1/2}} (\beta_h f' - g) = \frac{\xi}{\epsilon^2} \left(f' \frac{\partial g}{\partial \xi} - g' \frac{\partial f}{\partial \xi} \right), \end{aligned} \quad (2.12)$$

$$\frac{2-N}{2-2N} \omega'' + \frac{3}{4\epsilon} f \omega' - \frac{1}{4\epsilon} f' \omega - \frac{N}{1-N} \xi^{1/2} (2\omega + \frac{1}{\epsilon} f'') = \frac{\xi}{\epsilon} \left(f' \frac{\partial \omega}{\partial \xi} - \omega' \frac{\partial f}{\partial \xi} \right), \quad (2.13)$$

$$\frac{1}{Pr} \left(1 + \frac{4}{3} R_d \right) \theta'' + \frac{3}{4} f \theta' - \xi^{1/2} \frac{\delta}{Pr} \theta = \xi \left(f' \frac{\partial \theta}{\partial \xi} - \theta' \frac{\partial f}{\partial \xi} \right), \quad (2.14)$$

$$\frac{1}{Sc} \phi'' + \frac{3}{4} f \phi' - \xi^{1/2} K \phi = \xi \left(f' \frac{\partial \phi}{\partial \xi} - \phi' \frac{\partial f}{\partial \xi} \right), \quad (2.15)$$

where prime denotes differentiation with respect to η , $Re_L = \frac{U_\infty L}{\nu}$ is the local Reynolds number, $Ha = \frac{\sigma B_0^2 L^2}{\mu}$ is the Hartmann number, $D_a = \frac{K_p}{L^2}$ is the Darcy number, $F_s = \frac{b}{L}$ is the Forchheimer number, $N = \frac{\kappa}{\mu + \kappa}$ is the coupling number, $Pr = \frac{\nu \rho C_p}{\lambda}$ is the Prandtl number, $\delta = \frac{Q_0 \nu^2}{\lambda U_\infty^2}$ is the heat source/sink parameter, $Sc = \frac{\nu}{D}$ is the Schmidt number, $K = \frac{K_1 \nu}{U_\infty^2}$ is the chemical reaction parameter and $R_d = \frac{4\sigma T_\infty^3}{\chi \lambda}$ is the radiation parameter.

The boundary conditions take the form

$$f(\xi, 0) = -\frac{4}{3} \xi \frac{\partial f}{\partial \xi}(\xi, 0), \quad f'(\xi, 0) = 0, \quad g(\xi, 0) = 0, \quad (2.16)$$

$$\omega(\xi, 0) = -n f''(\xi, 0), \quad \theta(\xi, 0) = \phi(\xi, 0) = 1, \quad (2.17)$$

$$f'(\xi, \infty) = 1, \quad g(\xi, \infty) = \omega(\xi, \infty) = \theta(\xi, \infty) = \phi(\xi, \infty) = 0. \quad (2.18)$$

The non-dimensional skin friction, Nusselt and Sherwood numbers are respectively given by

$$C_{fx} Re_L^{1/2} = \left(\frac{2}{1-N} \right) f''(\xi, 0), \quad \frac{Nu_x}{Re_L^{1/2}} = -\theta'(\xi, 0), \quad \frac{Sh_x}{Re_L^{1/2}} = -\phi'(\xi, 0). \quad (2.19)$$

3. Method of solution

In this section, we introduce the OMD-BSLLM for approximating solutions of a system of nonlinear PDEs. Consider a system of n nonlinear PDEs of the form

$$\begin{aligned}\Gamma_1[F_1, F_2, \dots, F_n] &= 0, \\ \Gamma_2[F_1, F_2, \dots, F_n] &= 0, \\ &\vdots \\ \Gamma_n[F_1, F_2, \dots, F_n] &= 0,\end{aligned}\tag{3.1}$$

where the operators F_i ($i = 1, 2, 3, \dots, n$) are of the form

$$\begin{aligned}F_1 &= \left\{ g_1, \frac{\partial g_1}{\partial \eta}, \frac{\partial^2 g_1}{\partial \eta^2}, \dots, \frac{\partial^s g_1}{\partial \eta^s}, \frac{\partial g_1}{\partial \xi}, \frac{\partial}{\partial \xi} \left(\frac{\partial g_1}{\partial \eta} \right) \right\} \\ F_2 &= \left\{ g_2, \frac{\partial g_2}{\partial \eta}, \frac{\partial^2 g_2}{\partial \eta^2}, \dots, \frac{\partial^s g_2}{\partial \eta^s}, \frac{\partial g_2}{\partial \xi}, \frac{\partial}{\partial \xi} \left(\frac{\partial g_2}{\partial \eta} \right) \right\} \\ &\vdots \\ F_n &= \left\{ g_n, \frac{\partial g_n}{\partial \eta}, \frac{\partial^2 g_n}{\partial \eta^2}, \dots, \frac{\partial^s g_n}{\partial \eta^s}, \frac{\partial g_n}{\partial \xi}, \frac{\partial}{\partial \xi} \left(\frac{\partial g_n}{\partial \eta} \right) \right\},\end{aligned}\tag{3.2}$$

and $g_k(\eta, \xi)$ and Γ_k are non-linear operators containing spatial and time derivatives of $g_k(\eta, \xi)$. To apply OMD-BSLLM, the time interval $\xi \in [\xi_0, \xi_F]$ is decomposed into q non-overlapping sub-intervals defined as

$$J_v = (\xi_{v-1}, \xi_v), \quad v = 1, 2, 3, \dots, q,\tag{3.3}$$

where each J_v interval is discretised into $N_\xi + 1$ collocation points. The space interval $[a, b]$ is decomposed into p overlapping sub-intervals of length L , denoted by

$$I_\mu = [\eta_0^\mu, \eta_{N_\eta}^\mu], \quad \mu = 1, 2, 3, \dots, p,\tag{3.4}$$

where each I_μ interval is further discretized into $N_\eta + 1$ collocation points. Without loss of generality, we will consider that each sub-interval has the same length

$$L = \frac{b - a}{p + \frac{1}{2}(1 - p)(1 - \cos \frac{\pi}{N_\eta})}\tag{3.5}$$

for the overlap to be possible and the same number of collocation points is used in each subinterval. In the domain decomposition scheme, we use overlapping subintervals I_μ , where the first two points of the interval $I_{\mu+1}$ coincide with the last two points of the interval I_μ , that is $\eta_0^1 = a, \eta_{N_\eta}^p = b, \eta_{N_\eta-1}^\mu = \eta_0^{\mu+1}, \eta_{N_\eta}^\mu = \eta_1^{\mu+1}$. The domain decomposition in both the space and time intervals is shown in Figure 1.

The Chebyshev-Gauss-Lobatto points and the corresponding differentiation matrices [7, 34] are defined in the interval $[-1, 1]$. Therefore, before applying the spectral method on the sub-intervals, the time interval $\xi \in [\xi_{v-1}, \xi_v]$ and the space interval $\eta \in [\eta_0^\mu, \eta_{N_\eta}^\mu]$ are respectively transformed into $\tau \in [-1, 1]$ and $z \in [-1, 1]$ using the linear transformations

$$\xi_j = \frac{1}{2}(\xi_v - \xi_{v-1})\tau_j + \frac{1}{2}(\xi_v + \xi_{v-1}), \quad \tau_j = \cos \left(\frac{\pi j}{N_\xi} \right),\tag{3.6}$$

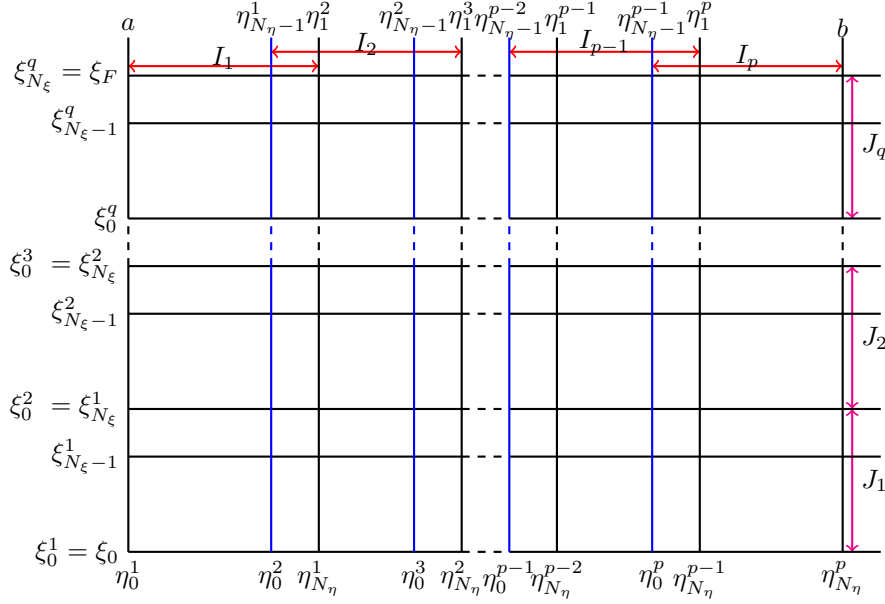


Figure 1. Overlapping and non-overlapping grid

$$\eta_i^\mu = \frac{L}{2}(z_i + 1), \quad z_i = \cos\left(\frac{\pi i}{N_\eta}\right). \quad (3.7)$$

We assume that at each sub-interval, the solution can be approximated by a bivariate Lagrange interpolation polynomial of the form

$$g_k^{(\mu,v)}(\eta, \xi) \approx \sum_{i=0}^{N_\eta} \sum_{j=0}^{N_\xi} g_k^{(\mu,v)}(z_i, \tau_j) \mathcal{L}_i(z) \mathcal{L}_j(\tau), \quad (3.8)$$

for $\mu = 1, 2, 3, \dots, p$ and $v = 1, 2, 3, \dots, q$. The function \mathcal{L}_i is the characteristic Lagrange cardinal polynomial based on the Chebyshev-Gauss-Lobatto points

$$\mathcal{L}_i(\eta) = \prod_{\substack{i=0 \\ i \neq k}}^{N_\eta} \frac{\eta - \eta_k}{\eta_i - \eta_k} \quad (3.9)$$

that satisfy the Kronecker delta equation

$$\mathcal{L}_i(\eta_k) = \delta_{ik} = \begin{cases} 0 & \text{if } i \neq k \\ 1 & \text{if } i = k \end{cases} \quad (3.10)$$

within the subdomain. The function \mathcal{L}_j is defined in a similar manner. Applying the quasilinearisation method gives

$$\begin{aligned} \Gamma_k[F_1, F_2, \dots, F_n] &\approx \Gamma_k[F_{1,r}, F_{2,r}, \dots, F_{n,r}] \\ &+ (F_{1,r+1} - F_{1,r}, F_{2,r+1} - F_{2,r}, \dots, F_{n,r+1} - F_{n,r}) \cdot \nabla \Gamma_k[F_{1,r}, F_{2,r}, \dots, F_{n,r}], \end{aligned} \quad (3.11)$$

where r and $r + 1$ denote previous and current iteration, respectively. The vector of the partial derivatives denoted by ∇ is defined as

$$\nabla = \{\nabla_{g_1}, \nabla_{g_2}, \dots, \nabla_{g_n}\}. \quad (3.12)$$

We define

$$\nabla_{g_1} = \left\{ \frac{\partial}{\partial g_1}, \frac{\partial}{\partial g_1'}, \frac{\partial}{\partial g_1''}, \dots, \frac{\partial}{\partial g_1^{(s)}}, \frac{\partial}{\partial \left(\frac{\partial g_1}{\partial \xi}\right)}, \frac{\partial}{\partial \left(\frac{\partial g_1'}{\partial \xi}\right)} \right\}, \quad (3.13)$$

$$\nabla_{g_2} = \left\{ \frac{\partial}{\partial g_2}, \frac{\partial}{\partial g_2'}, \frac{\partial}{\partial g_2''}, \dots, \frac{\partial}{\partial g_2^{(s)}}, \frac{\partial}{\partial \left(\frac{\partial g_2}{\partial \xi}\right)}, \frac{\partial}{\partial \left(\frac{\partial g_2'}{\partial \xi}\right)} \right\}, \quad (3.14)$$

\vdots

$$\nabla_{g_n} = \left\{ \frac{\partial}{\partial g_n}, \frac{\partial}{\partial g_n'}, \frac{\partial}{\partial g_n''}, \dots, \frac{\partial}{\partial g_n^{(s)}}, \frac{\partial}{\partial \left(\frac{\partial g_n}{\partial \xi}\right)}, \frac{\partial}{\partial \left(\frac{\partial g_n'}{\partial \xi}\right)} \right\}, \quad (3.15)$$

where the prime denotes differentiation with respect to η . The linearized equation (3.11) can be expressed as a system

$$\sum_{l=0}^s \alpha_{l,r}^{(\mu,v,1)} g_{1,r+1}^{(l,\mu,v)} + \beta_r^{(\mu,v,1)} \frac{\partial g_{1,r+1}^{(0,\mu,v)}}{\partial \xi} + \gamma_r^{(\mu,v,1)} \frac{\partial g_{1,r+1}^{(1,\mu,v)}}{\partial \xi} = R_1^{(\mu,v)}, \quad (3.16)$$

$$\sum_{l=0}^s \alpha_{l,r}^{(\mu,v,2)} g_{2,r+1}^{(l,\mu,v)} + \beta_r^{(\mu,v,2)} \frac{\partial g_{2,r+1}^{(0,\mu,v)}}{\partial \xi} + \gamma_r^{(\mu,v,2)} \frac{\partial g_{2,r+1}^{(1,\mu,v)}}{\partial \xi} = R_2^{(\mu,v)}, \quad (3.17)$$

\vdots

$$\sum_{l=0}^s \alpha_{l,r}^{(\mu,v,n)} g_{n,r+1}^{(l,\mu,v)} + \beta_r^{(\mu,v,n)} \frac{\partial g_{n,r+1}^{(0,\mu,v)}}{\partial \xi} + \gamma_r^{(\mu,v,n)} \frac{\partial g_{n,r+1}^{(1,\mu,v)}}{\partial \xi} = R_n^{(\mu,v)}, \quad (3.18)$$

where $\alpha_{l,r}^{(\mu,v,k)}(\eta, \xi)$, $\beta_r^{(\mu,v,k)}(\eta, \xi)$ and $\gamma_r^{(\mu,v,k)}(\eta, \xi)$ are variable coefficients of $g_{k,r+1}^{(l,\mu,v)}$, $\frac{\partial g_{k,r+1}^{(0,\mu,v)}}{\partial \xi}$, and $\frac{\partial g_{k,r+1}^{(1,\mu,v)}}{\partial \xi}$, respectively, for $k = 1, 2, \dots, n$ and $l = 0, 1, 2, \dots, s$. These variable coefficients correspond to the k^{th} equation, for $k = 1, 2, \dots, n$. Since constant s denotes the order of differentiation, then

$$\alpha_{l,r}^{(\mu,v,k)} = \frac{\partial \Gamma_k}{\partial g_{k,r}^{(l,\mu,v)}}, \quad \beta_r^{(\mu,v,k)} = \frac{\partial \Gamma_k}{\partial \left(\frac{\partial g_{k,r}^{(0,\mu,v)}}{\partial \xi}\right)}, \quad \gamma_r^{(\mu,v,k)} = \frac{\partial \Gamma_k}{\partial \left(\frac{\partial g_{k,r}^{(1,\mu,v)}}{\partial \xi}\right)}, \quad (3.19)$$

$$R_k^{(\mu,v)} = \sum_{l=0}^s \alpha_{l,r}^{(\mu,v,k)} g_{k,r}^{(l,\mu,v)} + \beta_r^{(\mu,v,k)} \frac{\partial g_{k,r}^{(0,\mu,v)}}{\partial \xi} + \gamma_r^{(\mu,v,k)} \frac{\partial g_{k,r}^{(1,\mu,v)}}{\partial \xi} - \Gamma_k. \quad (3.20)$$

Equations (3.16)–(3.18) are evaluated at the Chebyshev-Gauss-Lobatto grid points ξ_j ($j = 0, 1, 2, \dots, N_\xi$) and η_i ($i = 0, 1, 2, \dots, N_\eta$). The values of the time derivatives are computed at the Chebyshev-Gauss-Lobatto points as

$$\left. \frac{\partial g_n^{(\mu,v)}}{\partial \xi} \right|_{(z_\kappa, \tau_i)} = \left(\frac{2}{\xi_v - \xi_{v-1}} \right) \sum_{j=0}^{N_\xi} d_{i,j} g_n^{(\mu,v)}(z_\kappa, \tau_j) \quad (3.21)$$

$$= \left(\frac{2}{\xi_v - \xi_{v-1}} \right) \sum_{j=0}^{N_\xi} d_{i,j} \mathbf{G}_{n,j}^{(\mu,v)}. \quad (3.22)$$

The values of the first, second and higher sth order space derivatives are computed as

$$\left. \frac{\partial g_n^{(\mu,v)}}{\partial \eta} \right|_{(z_\kappa, \tau_i)} = \frac{2}{\eta_{N_\eta}^\mu - \eta_0^\mu} \sum_{\nu=0}^{N_\eta} D_{\kappa,\nu}^{(\mu)} g_n^{(\mu,v)}(z_\nu, \tau_i), \quad (3.23)$$

$$\left. \frac{\partial^2 g_n^{(\mu,v)}}{\partial \eta^2} \right|_{(z_\kappa, \tau_i)} = \left(\frac{2}{\eta_{N_\eta}^\mu - \eta_0^\mu} \right)^2 \sum_{\nu=0}^{N_\eta} \left[D_{\kappa,\nu}^{(\mu)} \right]^2 g_n^{(\mu,v)}(z_\nu, \tau_i), \quad (3.24)$$

$$\left. \frac{\partial^s g_n^{(\mu,v)}}{\partial \eta^s} \right|_{(z_\kappa, \tau_i)} = \left(\frac{2}{\eta_{N_\eta}^\mu - \eta_0^\mu} \right)^s \sum_{\nu=0}^{N_\eta} \left[D_{\kappa,\nu}^{(\mu)} \right]^s g_n^{(\mu,v)}(z_\nu, \tau_i) = \left[\mathbf{D}^{(\mu)} \right]^s \mathbf{G}_{n,i}^{(\mu,v)}, \quad (3.25)$$

where the vector $\mathbf{G}_{n,i}^{(\mu,v)}$ is defined as

$$\mathbf{G}_{n,i}^{(\mu,v)} = \left[g_n^{(\mu,v)}(\eta_0^\mu, \xi_i^{(v)}), g_n^{(\mu,v)}(\eta_1^\mu, \xi_i^{(v)}), g_n^{(\mu,v)}(\eta_2^\mu, \xi_i^{(v)}), \dots, g_n^{(\mu,v)}(\eta_{N_\eta}^\mu, \xi_i^{(v)}) \right]^T \quad (3.26)$$

and T denotes matrix transpose. Substituting equations (3.21)–(3.25) into equations (3.16)–(3.18) yields

$$A_{1,1}^{(\mu,v)} \mathbf{G}_{1,i,r+1}^{(\mu,v)} + \beta_r^{(\mu,v,1)} \sum_{j=0}^{N_\xi} d_{i,j} \mathbf{G}_{1,j}^{(\mu,v)} + \gamma_r^{(\mu,v,1)} \sum_{j=0}^{N_\xi} d_{i,j} \mathbf{D}^{(\mu)} \mathbf{G}_{1,j}^{(\mu,v)} = \mathbf{R}_{1,i}^{(\mu,v)} \quad (3.27)$$

$$A_{2,2}^{(\mu,v)} \mathbf{G}_{2,i,r+1}^{(\mu,v)} + \beta_r^{(\mu,v,2)} \sum_{j=0}^{N_\xi} d_{i,j} \mathbf{G}_{2,j}^{(\mu,v)} + \gamma_r^{(\mu,v,2)} \sum_{j=0}^{N_\xi} d_{i,j} \mathbf{D}^{(\mu)} \mathbf{G}_{2,j}^{(\mu,v)} = \mathbf{R}_{2,i}^{(\mu,v)} \quad (3.28)$$

⋮

$$A_{n,n}^{(\mu,v)} \mathbf{G}_{n,i,r+1}^{(\mu,v)} + \beta_r^{(\mu,v,n)} \sum_{j=0}^{N_\xi} d_{i,j} \mathbf{G}_{n,j}^{(\mu,v)} + \gamma_r^{(\mu,v,n)} \sum_{j=0}^{N_\xi} d_{i,j} \mathbf{D}^{(\mu)} \mathbf{G}_{n,j}^{(\mu,v)} = \mathbf{R}_{n,i}^{(\mu,v)} \quad (3.29)$$

where

$$A_{1,1}^{(\mu,v)} = \sum_{l=0}^s \alpha_{l,r}^{(\mu,v,1)} \left[\mathbf{D}^{(\mu)} \right]^l, \dots, A_{n,n}^{(\mu,v)} = \sum_{l=0}^s \alpha_{l,r}^{(\mu,v,n)} \left[\mathbf{D}^{(\mu)} \right]^l,$$

Imposing the boundary conditions, equations (3.27)–(3.29) become

$$A_{1,1}^{(\mu,v)} \mathbf{G}_{1,i,r+1}^{(\mu,v)} + \beta_r^{(\mu,v,1)} \sum_{j=0}^{N_\xi-1} d_{i,j} \mathbf{G}_{1,j}^{(\mu,v)} + \gamma_r^{(\mu,v,1)} \sum_{j=0}^{N_\xi-1} d_{i,j} \mathbf{D}^{(\mu)} \mathbf{G}_{1,j}^{(\mu,v)} = \mathbf{K}_{1,i}^{(\mu,v)} \quad (3.30)$$

$$A_{2,2}^{(\mu,v)} \mathbf{G}_{2,i,r+1}^{(\mu,v)} + \beta_r^{(\mu,v,2)} \sum_{j=0}^{N_\xi-1} d_{i,j} \mathbf{G}_{2,j}^{(\mu,v)} + \gamma_r^{(\mu,v,2)} \sum_{j=0}^{N_\xi-1} d_{i,j} \mathbf{D}^{(\mu)} \mathbf{G}_{2,j}^{(\mu,v)} = \mathbf{K}_{2,i}^{(\mu,v)} \quad (3.31)$$

⋮

$$A_{n,n}^{(\mu,v)} \mathbf{G}_{n,i,r+1}^{(\mu,v)} + \beta_r^{(\mu,v,n)} \sum_{j=0}^{N_\xi-1} d_{i,j} \mathbf{G}_{n,j}^{(\mu,v)} + \gamma_r^{(\mu,v,n)} \sum_{j=0}^{N_\xi-1} d_{i,j} \mathbf{D}^{(\mu)} \mathbf{G}_{n,j}^{(\mu,v)} = \mathbf{K}_{n,i}^{(\mu,v)} \quad (3.32)$$

where

$$\mathbf{K}_{1,i}^{(\mu,v)} = \mathbf{R}_{1,i}^{(\mu,v)} - \beta_r^{(\mu,v,1)} d_{i,N_\xi} \mathbf{G}_{1,N_\xi}^{(\mu,v)} - \gamma_r^{(\mu,v,1)} d_{i,N_\xi} \mathbf{D}^{(\mu)} \mathbf{G}_{1,N_\xi}^{(\mu,v)}, \quad (3.33)$$

$$\mathbf{K}_{2,i}^{(\mu,v)} = \mathbf{R}_{2,i}^{(\mu,v)} - \beta_r^{(\mu,v,2)} d_{i,N_\xi} \mathbf{G}_{2,N_\xi}^{(\mu,v)} - \gamma_r^{(\mu,v,2)} d_{i,N_\xi} \mathbf{D}^{(\mu)} \mathbf{G}_{2,N_\xi}^{(\mu,v)}, \quad (3.34)$$

⋮

$$\mathbf{K}_{n,i}^{(\mu,v)} = \mathbf{R}_{n,i}^{(\mu,v)} - \beta_r^{(\mu,v,n)} d_{i,N_\xi} \mathbf{G}_{n,N_\xi}^{(\mu,v)} - \gamma_r^{(\mu,v,n)} d_{i,N_\xi} \mathbf{D}^{(\mu)} \mathbf{G}_{n,N_\xi}^{(\mu,v)}. \quad (3.35)$$

Each equation from (3.30) - (3.32) can be converted into a matrix system:

$$\mathbf{A} \Omega_{i,r+1}^{(\mu,v)} = \mathbf{K}_{\varepsilon,r+1}^{(\mu,v)}, \quad (3.36)$$

where $\Omega = \{\mathbf{G}_1, \mathbf{G}_2, \dots, \mathbf{G}_n\}$ and $\varepsilon = \{1, 2, 3, \dots, n\}$. The size of matrix \mathbf{A} is $(M + 1) \times (M + 1)$, where $M = N_\eta + (N_\eta - 1)(p - 1)$, is the total number of collocation points over a single domain $[-1, 1]$. The coefficient of matrix \mathbf{A} has the structure

$$\left[\begin{array}{cccccccc} A_{0,0}^{(p)} & A_{0,1}^{(p)} & \cdots & A_{0,N_\eta-1}^{(p)} & A_{0,N_\eta}^{(p)} & & & \\ A_{1,0}^{(p)} & A_{1,1}^{(p)} & \cdots & A_{1,N_\eta-1}^{(p)} & A_{1,N_\eta}^{(p)} & & & \\ \vdots & \vdots & \ddots & \vdots & \vdots & & & \\ A_{N_\eta-1,0}^{(p)} & A_{N_\eta-1,1}^{(p)} & \cdots & A_{N_\eta-1,N_\eta-1}^{(p)} & A_{N_\eta-1,N_\eta}^{(p)} & & & \\ & & & A_{1,0}^{(p-1)} & A_{1,1}^{(p-1)} & \cdots & A_{1,N_\eta-1}^{(p-1)} & A_{1,N_\eta}^{(p-1)} \\ & & & A_{2,0}^{(p-1)} & A_{2,1}^{(p-1)} & \cdots & A_{2,N_\eta-1}^{(p-1)} & A_{2,N_\eta}^{(p-1)} \\ & & & \vdots & \vdots & \ddots & \vdots & \vdots \\ & & & A_{N_\eta-1,0}^{(p-1)} & A_{N_\eta-1,1}^{(p-1)} & \cdots & A_{N_\eta-1,N_\eta-1}^{(p-1)} & A_{N_\eta-1,N_\eta}^{(p-1)} \\ & & & & & & \vdots & \vdots \\ & & & & & & A_{1,0}^{(1)} & A_{1,1}^{(1)} & \cdots & A_{1,N_\eta-1}^{(1)} & A_{1,N_\eta}^{(1)} \\ & & & & & & A_{2,0}^{(1)} & A_{2,1}^{(1)} & \cdots & A_{2,N_\eta-1}^{(1)} & A_{2,N_\eta}^{(1)} \\ & & & & & & \vdots & \vdots & \ddots & \vdots & \vdots \\ & & & & & & A_{N_\eta,0}^{(1)} & A_{N_\eta,1}^{(1)} & \cdots & A_{N_\eta,N_\eta-1}^{(1)} & A_{N_\eta,N_\eta}^{(1)} \end{array} \right] \quad (3.37)$$

Since the highest order of differentiation for equations (2.11)–(2.15) is $s = 3$ and $n = 5$, applying OMD-Bsllm method to the equations, we obtain

$$A_{1,1}^{(\mu,v)} \mathbf{G}_{1,i}^{(\mu,v)} + \beta_r^{(\mu,v,1)} \sum_{j=0}^{N_\xi} d_{i,j} \mathbf{G}_{1,j}^{(\mu,v)} + \gamma_r^{(\mu,v,1)} \sum_{j=0}^{N_\xi} d_{i,j} \mathbf{D}^{(\mu)} \mathbf{G}_{1,j}^{(\mu,v)} = \mathbf{R}_{1,i}^{(\mu,v)}, \quad (3.38)$$

$$A_{2,2}^{(\mu,v)} \mathbf{G}_{2,i}^{(\mu,v)} + \beta_r^{(\mu,v,2)} \sum_{j=0}^{N_\xi} d_{i,j} \mathbf{G}_{2,j}^{(\mu,v)} + \gamma_r^{(\mu,v,2)} \sum_{j=0}^{N_\xi} d_{i,j} \mathbf{D}^{(\mu)} \mathbf{G}_{2,j}^{(\mu,v)} = \mathbf{R}_{2,i}^{(\mu,v)}, \quad (3.39)$$

$$A_{3,3}^{(\mu,v)} \mathbf{G}_{3,i}^{(\mu,v)} + \beta_r^{(\mu,v,3)} \sum_{j=0}^{N_\xi} d_{i,j} \mathbf{G}_{3,j}^{(\mu,v)} + \gamma_r^{(\mu,v,3)} \sum_{j=0}^{N_\xi} d_{i,j} \mathbf{D}^{(\mu)} \mathbf{G}_{3,j}^{(\mu,v)} = \mathbf{R}_{3,i}^{(\mu,v)}, \quad (3.40)$$

$$A_{4,4}^{(\mu,v)} \mathbf{G}_{4,i}^{(\mu,v)} + \beta_r^{(\mu,v,4)} \sum_{j=0}^{N_\xi} d_{i,j} \mathbf{G}_{4,j}^{(\mu,v)} + \gamma_r^{(\mu,v,4)} \sum_{j=0}^{N_\xi} d_{i,j} \mathbf{D}^{(\mu)} \mathbf{G}_{4,j}^{(\mu,v)} = \mathbf{R}_{4,i}^{(\mu,v)}, \quad (3.41)$$

$$A_{5,5}^{(\mu,v)} \mathbf{G}_{5,i}^{(\mu,v)} + \beta_r^{(\mu,v,5)} \sum_{j=0}^{N_\xi} d_{i,j} \mathbf{G}_{5,j}^{(\mu,v)} + \gamma_r^{(\mu,v,5)} \sum_{j=0}^{N_\xi} d_{i,j} \mathbf{D}^{(\mu)} \mathbf{G}_{5,j}^{(\mu,v)} = \mathbf{R}_{5,i}^{(\mu,v)}, \quad (3.42)$$

where

$$A_{1,1}^{(\mu,v)} = \sum_l^3 \alpha_{l,r}^{(\mu,v,1)} [\mathbf{D}^{(\mu)}]^l, A_{2,2}^{(\mu,v)} = \sum_l^3 \alpha_{l,r}^{(\mu,v,2)} [\mathbf{D}^{(\mu)}]^l, A_{3,3}^{(\mu,v)} = \sum_l^3 \alpha_{l,r}^{(\mu,v,3)} [\mathbf{D}^{(\mu)}]^l, \\ A_{4,4}^{(\mu,v)} = \sum_l^3 \alpha_{l,r}^{(\mu,v,4)} [\mathbf{D}^{(\mu)}]^l, A_{5,5}^{(\mu,v)} = \sum_l^3 \alpha_{l,r}^{(\mu,v,5)} [\mathbf{D}^{(\mu)}]^l.$$

To apply our method, we let $f(\eta, \xi) = g_1(\eta, \xi)$, $g(\eta, \xi) = g_2(\eta, \xi)$, $\omega(\eta, \xi) = g_3(\eta, \xi)$, $\theta(\eta, \xi) = g_4(\eta, \xi)$ and $\phi(\eta, \xi) = g_5(\eta, \xi)$. Therefore, we have

$$\Gamma_1 = \frac{1}{\epsilon(1-N)} g_{1,r}^{(3,\mu,v)} + \frac{3}{4\epsilon^2} g_{1,r}^{(0,\mu,v)} g_{1,r}^{(2,\mu,v)} - \left(\frac{1}{2\epsilon^2} + \xi \frac{Fs}{Da} \right) \left(g_{1,r}^{(1,\mu,v)} \right)^2 + \lambda g_{4,r}^{(0,\mu,v)} \\ - \left(\frac{N}{1-N} \right) g_{2,r}^{(1,\mu,v)} + g_{3,r}^{(0,\mu,v)} - \frac{\xi^{\frac{1}{2}}}{Da Re_L^{1/2}} g_{1,r}^{(1,\mu,v)} - \frac{\xi^{\frac{1}{2}} Ha^2}{\epsilon(1+\beta_h^2) Re_L^{1/2}} g_{1,r}^{(1,\mu,v)} \\ - \frac{\xi^{\frac{1}{2}} \beta_h Ha^2}{\epsilon(1+\beta_h^2) Re_L^{1/2}} g_{2,r}^{(0,\mu,v)} - \frac{\xi}{\epsilon^2} \left(g_{1,r}^{(1,\mu,v)} \frac{\partial g_{1,r}^{(1,\mu,v)}}{\partial \xi} - g_{1,r}^{(2,\mu,v)} \frac{\partial g_{1,r}^{(0,\mu,v)}}{\partial \xi} \right), \quad (3.43)$$

$$\Gamma_2 = \frac{1}{\epsilon(1-N)} g_{2,r}^{(2,\mu,v)} + \frac{3}{4\epsilon^2} g_{1,r}^{(0,\mu,v)} g_{2,r}^{(1,\mu,v)} - \frac{1}{2\epsilon^2} g_{2,r}^{(0,\mu,v)} g_{1,r}^{(1,\mu,v)} - \xi \frac{Fs}{Da} \left(g_{2,r}^{(0,\mu,v)} \right)^2 \\ - \frac{\xi^{1/2}}{Da Re_L^{1/2}} g_{2,r}^{(0,\mu,v)} + \frac{\xi^{1/2} Ha^2}{\epsilon(1+\beta_h^2) Re_L^{1/2}} (\beta_h g_{1,r}^{(1,\mu,v)} - g_{2,r}^{(0,\mu,v)}) \\ - \frac{\xi}{\epsilon^2} \left(g_{1,r}^{(1,\mu,v)} \frac{\partial g_{2,r}^{(0,\mu,v)}}{\partial \xi} - g_{2,r}^{(1,\mu,v)} \frac{\partial g_{1,r}^{(0,\mu,v)}}{\partial \xi} \right), \quad (3.44)$$

$$\Gamma_3 = \frac{2-N}{2-2N} g_{3,r}^{(2,\mu,v)} + \frac{3}{4\epsilon} g_{1,r}^{(0,\mu,v)} g_{3,r}^{(1,\mu,v)} - \left(\frac{N}{1-N} \right) \xi^{\frac{1}{2}} (2g_{3,r}^{(0,\mu,v)} + \frac{1}{\epsilon} g_{1,r}^{(2,\mu,v)}) \\ - \frac{1}{4\epsilon} g_{1,r}^{(1,\mu,v)} g_{3,r}^{(0,\mu,v)} - \frac{\xi}{\epsilon} \left(g_{1,r}^{(1,\mu,v)} \frac{\partial g_{3,r}^{(0,\mu,v)}}{\partial \xi} - g_{3,r}^{(1,\mu,v)} \frac{\partial g_{1,r}^{(0,\mu,v)}}{\partial \xi} \right), \quad (3.45)$$

$$\Gamma_4 = \frac{1}{Pr} \left(1 + \frac{4}{3} Rd \right) g_{4,r}^{(2,\mu,v)} + \frac{3}{4} g_{1,r}^{(0,\mu,v)} g_{4,r}^{(1,\mu,v)} - \xi^{\frac{1}{2}} \frac{\delta}{Pr} g_{4,r}^{(0,\mu,v)} \\ - \xi \left(g_{1,r}^{(1,\mu,v)} \frac{\partial g_{4,r}^{(0,\mu,v)}}{\partial \xi} - g_{4,r}^{(1,\mu,v)} \frac{\partial g_{1,r}^{(0,\mu,v)}}{\partial \xi} \right), \quad (3.46)$$

$$\Gamma_5 = \frac{1}{Sc} g_{5,r}^{(2,\mu,v)} + \frac{3}{4} g_{1,r}^{(0,\mu,v)} g_{5,r}^{(1,\mu,v)} - \xi^{\frac{1}{2}} K g_{5,r}^{(0,\mu,v)} \\ - \xi \left(g_{1,r}^{(1,\mu,v)} \frac{\partial g_{5,r}^{(0,\mu,v)}}{\partial \xi} - g_{5,r}^{(1,\mu,v)} \frac{\partial g_{1,r}^{(0,\mu,v)}}{\partial \xi} \right). \quad (3.47)$$

The variable coefficients for $s = 0, 1, 2, 3$ are given by

$$\begin{aligned}
\alpha_{3,r}^{(1,\mu,v)} &= \frac{1}{\epsilon(1-N)}, \quad \alpha_{2,r}^{(1,\mu,v)} = \frac{3}{4\epsilon^2}g_{1,r}^{(0,\mu,v)} + \frac{\xi}{\epsilon^2}\frac{\partial g_{1,r}^{(0,\mu,v)}}{\partial \xi}, \quad \alpha_{0,r}^{(1,\mu,v)} = \frac{3}{4\epsilon^2}g_{1,r}^{(2,\mu,v)}, \\
\alpha_{1,r}^{(1,\mu,v)} &= -\frac{1}{\epsilon^2}g_{1,r}^{(1,\mu,v)} - \frac{\xi^{\frac{1}{2}}Ha^2}{\epsilon(1+\beta_h^2)Re_L^{\frac{1}{2}}} - \frac{\xi^{\frac{1}{2}}}{DaRe_L^{\frac{1}{2}}} - 2\frac{\xi Fs}{Da}g_{1,r}^{(1,\mu,v)} - \frac{\xi}{\epsilon^2}\frac{\partial g_{1,r}^{(1,\mu,v)}}{\partial \xi}, \\
\alpha_{2,r}^{(2,\mu,v)} &= \frac{1}{\epsilon(1-N)}, \quad \alpha_{1,r}^{(2,\mu,v)} = \frac{3}{4\epsilon^2}g_{1,r}^{(0,\mu,v)} + \frac{\xi}{\epsilon^2}\frac{\partial g_{1,r}^{(0,\mu,v)}}{\partial \xi}, \\
\alpha_{0,r}^{(2,\mu,v)} &= -\frac{1}{2\epsilon^2}g_{1,r}^{(1,\mu,v)} - \frac{\xi^{\frac{1}{2}}}{DaRe_L^{\frac{1}{2}}} - 2\frac{\xi Fs}{Da}g_{2,r}^{(0,\mu,v)} - \frac{\xi^{\frac{1}{2}}Ha^2}{\epsilon(1+\beta_h^2)Re_L^{\frac{1}{2}}}, \\
\alpha_{2,r}^{(3,\mu,v)} &= \frac{2-N}{2-2N}, \quad \alpha_{1,r}^{(3,\mu,v)} = \frac{3}{4\epsilon}g_{1,r}^{(0,\mu,v)} + \frac{\xi}{\epsilon}\frac{\partial g_{1,r}^{(0,\mu,v)}}{\partial \xi}, \\
\alpha_{0,r}^{(3,\mu,v)} &= -\frac{1}{4\epsilon}g_{1,r}^{(1,\mu,v)} - \frac{2N\xi^{\frac{1}{2}}}{1-N}, \quad \alpha_{2,r}^{(4,\mu,v)} = \frac{1}{Pr}\left(1 + \frac{4}{3}Rd\right), \\
\alpha_{1,r}^{(4,\mu,v)} &= \frac{3}{4}g_{1,r}^{(0,\mu,v)} + \xi\frac{\partial g_{1,r}^{(0,\mu,v)}}{\partial \xi}, \quad \alpha_{0,r}^{(4,\mu,v)} = -\frac{\xi^{\frac{1}{2}}\delta}{Pr}, \quad \alpha_{2,r}^{(5,\mu,v)} = \frac{1}{Sc}, \\
\alpha_{1,r}^{(5,\mu,v)} &= \frac{3}{4}g_{1,r}^{(0,\mu,v)} + \xi\frac{\partial g_{1,r}^{(0,\mu,v)}}{\partial \xi}, \quad \alpha_{0,r}^{(5,\mu,v)} = -\xi^{\frac{1}{2}}K\beta_r^{(1,\mu,v)} = \frac{\xi}{4\epsilon^2}g_{1,r}^{(2,\mu,v)}, \\
\beta_r^{(2,\mu,v)} &= -\frac{\xi}{4\epsilon^2}g_{1,r}^{(1,\mu,v)}, \quad \beta_r^{(2,\mu,v)} = -\frac{\xi}{\epsilon}g_{1,r}^{(1,\mu,v)}, \quad \beta_r^{(3,\mu,v)} = -\frac{\xi}{4\epsilon}g_{1,r}^{(1,\mu,v)}, \\
\beta_r^{(4,\mu,v)} &= -\xi g_{1,r}^{(1,\mu,v)}, \quad \beta_r^{(5,\mu,v)} = -\xi g_{1,r}^{(1,\mu,v)}, \quad \gamma_r^{(1,\mu,v)} = -\frac{\xi}{4\epsilon^2}g_{1,r}^{(1,\mu,v)}, \\
\gamma_r^{(2,\mu,v)} &= \gamma_r^{(3,\mu,v)} = \gamma_r^{(4,\mu,v)} = \gamma_r^{(5,\mu,v)} = 0
\end{aligned}$$

and the right hand side for $k = 1, 2, 3, 4, 5$ is given by

$$R_{k,i}^{(\mu,v)} = \sum_{l=0}^3 \alpha_{l,r}^{(\mu,v,k)} g_{k,r}^{(1,\mu,v)} + \beta_r^{(\mu,v,k)} \frac{\partial g_{k,r}^{(0,\mu,v)}}{\partial \xi} + \gamma_r^{(\mu,v,k)} \frac{\partial g_{k,r}^{(1,\mu,v)}}{\partial \xi} - \Gamma_k. \quad (3.48)$$

Imposing the boundary conditions, equations (3.38)–(3.42) can be expressed as a matrix system of the form given in equation (3.36).

4. Results and discussion

The set of coupled dimensionless PDEs (2.11)–(2.15) along with the boundary conditions (2.16)–(2.18) have been solved numerically using the OMD-BSLLM. The edge of the boundary layer has been taken as $\eta_\infty = 20$ and the number of collocation points used in space and time are $N_\eta = 20$ and $N_\xi = 5$, respectively. In order to get a physical sense of the dynamics of the flow, a parametric study was undertaken to determine the effects of different parameters namely the radiation parameter Rd , the heat source/sink δ , the chemical reaction parameter K , the Forchheimer number Fs , Hartman number Ha , the coupling number N and the Hall parameter β_h on the fluid properties and flow characteristics. In

the entire numerical computations, we have chosen the following parameter values $\epsilon = 0.6, \delta = 0.5, N = 0.6, Pr = 0.72, Sc = 0.22, Da = 10, Rd = 0.3, Fs = Ha = 0.1, K = \beta_h = \lambda = 0.5, Re_L^{1/2} = n = 1$. The fluid properties for different values of the main controlling parameters are considered for the concentrated particle flows ($n = 0$) and the flow characteristics are considered for the turbulent boundary layer flows ($n = 1$). The numerical solutions obtained are tested for convergence and accuracy using both the convergence error norms and the residual errors. The errors are defined using the l_∞ norm. The convergence error norm is the difference between successive approximations, while the residual error quantifies the extent to which the solutions are approximated. The residual errors in the solutions $f(\xi, \eta), g(\xi, \eta), \omega(\xi, \eta), \theta(\xi, \eta)$ and $\phi(\xi, \eta)$ at each ξ are defined approximately as

$$Res(\psi) = \|\Delta_\psi [\mathbf{F}_{r+1,i}^{(\mu,v)}, \mathbf{G}_{r+1,i}^{(\mu,v)}, \mathbf{\Omega}_{r+1,i}^{(\mu,v)}, \mathbf{\Theta}_{r+1,i}^{(\mu,v)}, \mathbf{\Phi}_{r+1,i}^{(\mu,v)}]\|_\infty, \psi = \{f, g, \omega, \theta, \phi\}, \quad (4.1)$$

and the convergence error norms are defined as

$$E_\psi = \|\Psi_{r+1,i}^{(\mu,v)} - \Psi_{r,i}^{(\mu,v)}\|_\infty, \Psi^{(\mu,v)} = \{\mathbf{F}^{(\mu,v)}, \mathbf{G}^{(\mu,v)}, \mathbf{\Omega}^{(\mu,v)}, \mathbf{\Theta}^{(\mu,v)}, \mathbf{\Phi}^{(\mu,v)}\}, \quad (4.2)$$

where $i = 0, 1, 2, \dots, N_\xi$, Δ_ψ represent the nonlinear PDEs. The convergence error norms and the residual errors for the solutions $f(\xi, \eta), g(\xi, \eta), \omega(\xi, \eta), \theta(\xi, \eta)$ and $\phi(\xi, \eta)$ when $\xi = 1$ are shown in Figure 2. The errors decrease rapidly with an increase in the number of iterations. This is an indication that the numerical scheme converges. From Figure 2 (a) the OMD-BSLLM converges after 7 iterations and the size of the error is between 10^{-10} and 10^{-14} . We observe in Figure 2(b) that the results are consistent and the residual error is in the range 10^{-10} to 10^{-12} after 5 iterations. This analysis of the convergence and accuracy of the method of solution show that we can trust the numerical solutions obtained using the OMD-BSLLM. For validation of the method, our numerical results of the skin friction and heat transfer rate are compared with previously published results [9,10,17,36] for the case when $\epsilon = 1, \delta = N = \lambda = Rd = Ha = Fs = Sc = K = \beta_h = \xi = n = 0, Da \rightarrow \infty$. The comparison is shown in Tables 1 and 2. The results are found to be in excellent agreement.

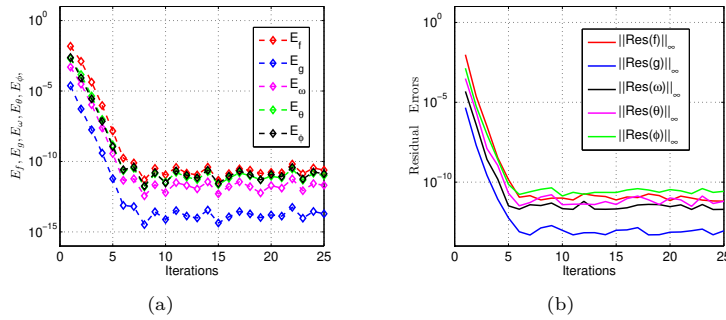


Figure 2. Error norms and residual errors against the number of iterations

Figure 3 illustrates the effect of the heat source/sink parameter and thermal radiation parameter on the temperature profiles. From Figure 3(a) we observe a

Table 1. Comparison of numerical values of $f''(0, 0)$ at different values of Pr .

Pr	Yih [36]	Chamkha [10]	Chamkha et al. [9]	Elbashbeshy et al. [17]	Present results
0.0001	1.4998	1.4997	1.4997	-	1.4998031
0.001	1.4728	1.4727	1.4727	-	1.4728521
0.01	1.3968	1.3965	1.3965	-	1.3967946
0.1	1.2104	1.2151	1.2151	1.2151	1.2152609
1	0.9084	0.9081	0.9081	0.9082	0.9081912
10	0.5927	0.5927	0.5927	0.5928	0.5928323
100	0.3559	0.3558	0.3558	-	0.3559337
1000	0.2049	0.2049	0.2049	-	0.2049424
10000	0.1161	0.1161	0.1161	-	0.1162981

Table 2. Comparison of numerical values of $-\theta'(0, 0)$ at different values of Pr .

Pr	Yih [36]	Chamkha [10]	Chamkha et al. [9]	Elbashbeshy et al. [17]	Present results
0.0001	0.0060	0.0059	0.0059	-	0.0059186
0.001	0.0189	0.0188	0.0188	-	0.01889173
0.01	0.0570	0.0574	0.0574	-	0.0573601
0.1	0.1629	0.1630	0.1630	0.1627	0.1627577
1	0.4012	0.4012	0.4012	0.4010	0.4010331
10	0.8266	0.8274	0.8274	0.8268	0.8268430
100	1.5493	0.5503	0.5503	-	1.5494888
1000	2.8035	2.8044	2.8044	-	2.8035516
10000	5.0127	5.0131	5.0131	-	5.0270365

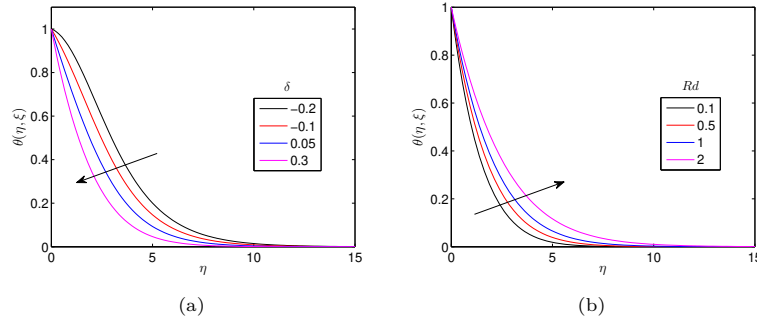


Figure 3. Effect of δ and Rd on temperature

reduction in the temperature of the micropolar fluid flow due to an increase in the strength of heat generation ($\delta > 0$). From the same figure, we note that the temperature of the micropolar fluid flow increases due to an increase of the heat absorption ($\delta < 0$) strength. The same results were observed by Ahmad [4]. Physically speaking, the presence of the heat generation coefficient tends to reduce the micropolar fluid temperature. This causes the thermal buoyancy effects to decrease resulting in a net reduction in the temperature in the domain. The opposite is true for the heat absorption parameter. It is also observed from the figure that the thermal boundary layer thickness decreases as the heat generation coefficient increases, whereas is enhanced with the heat absorption coefficient. Generally, the temperature profile is expected to increase with increasing values of heat generation and decrease with heat absorption, but due to the domination of the external temperature, the

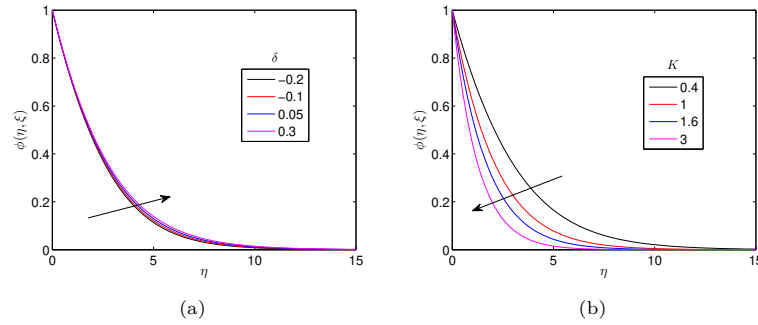


Figure 4. Effect of δ and K on concentration

opposite results to that of expected are noted. The effect of the thermal radiation parameter on the temperature distribution across the boundary layer is presented in Figure 3(b). The increment in thermal radiation is seen to give more heat to the fluid which results in a rise in the dimensionless temperature in the boundary layer. Moreover, the thermal boundary layer thickness is enhanced with greater values of the thermal radiation parameter. The thermal boundary layer is energized with greater radiative flux contribution which leads to high fluid temperature.

The influence of the heat source/sink parameter and chemical reaction parameter on the concentration profiles is depicted in Figure 4. Figure 4(a) shows that the effect of heat source/sink on the concentration distribution is less significant in the micropolar fluid flow. Generally, the concentration profiles move to cooler areas when external heat to the flow is produced. Since the heat source/sink act like heat observer, the heat generation increases the concentration and the heat absorption reduces the concentration profiles as shown in Figure 4(a). It is seen in Figure 4(b) that increasing the chemical reaction parameter causes a decrease in the concentration of the micropolar fluid flow along the surface due to the thinning of the solutal boundary layer thickness.

Figures 5–7 depict the effects of the coupling number, thermal radiation parameter, chemical reaction parameter, heat source/sink parameter, Forchheimer number and Hartman number on the microrotation profiles. We observe that the microrotation changes in sign from negative to positive within the boundary layer. The striking feature of the distribution is that at approximately $\eta = 3$, where the profiles intersect each other suggesting the reverse effect for $\eta > 3$. This observation concurs with findings reported by Srinivashacharya and Mendu [33]. The angular velocity satisfies the boundary conditions (2.7)–(2.8) since the microrotation takes the negative values of the gradient of velocity at the plate surface and approach zero away from the plate surface.

Figure 5 exhibits the effects of the coupling number and thermal radiation parameter on the microrotation profiles. It is seen from Figure 5(a) that the magnitude of microrotation decreases near the surface and increases far away from the wall with increasing values of the coupling number. The coupling number characterises the coupling of linear and rotational motion arising from the micromotion of the fluid motion. Thus, the coupling number signifies the coupling between the Newtonian and rotational viscosities. From the figure, we observe that the microrotation tends to zero as is expected that in the limit $\kappa \rightarrow 0$ i.e $N \rightarrow 0$ the micropolarity is lost

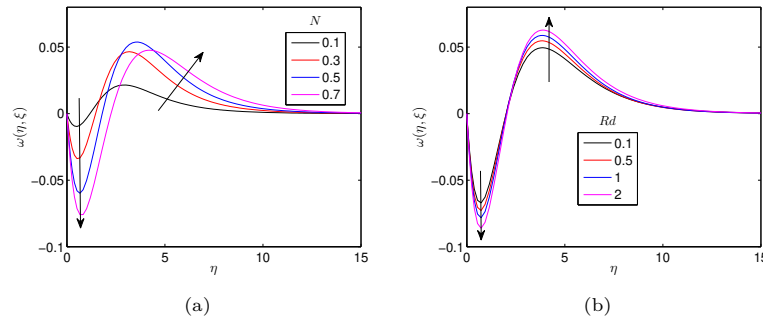


Figure 5. Effect of N and Rd on microrotation

and the fluid behaves as a non-polar fluid, and equation (2.11) and (2.13) decoupled and reduce to viscous fluid flow equations. It is also noted that that as the coupling number increases, the effect of microstructure becomes significant, whereas with diminishing values of the coupling number small microrotation is generated. Figure 5(b) shows that the magnitude of microrotation decreases near the vertical plate and rises away from the plate with increasing thermal radiation parameter. The microrotation component is enhanced because when the intensity of heat generated through thermal radiation increases, the bond holding the components of the fluid particle is easily broken and the fluid velocity will increase. We also observe from the figure that the higher the value of the thermal radiation parameter, the higher the thermal boundary layer thickness.

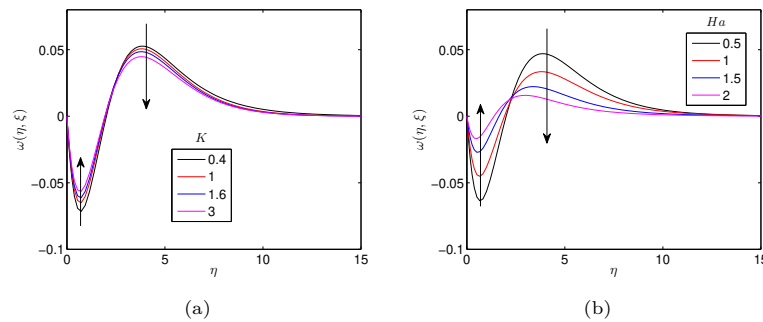


Figure 6. Effect of K and Ha on microrotation

Figure 6 depicts that the microrotation component increases with increasing values of the chemical reaction parameter and Hartman number near the plate, but away from the plate the reverse effect is encountered. It is observed from Figure 6(a) that the presence of the magnetic force causes retardation of the fluid motion represented by a general decrease in the fluid angular velocity (except near the wall). The decrease in microrotation due to the chemical reaction parameter and Hartman number in the free stream was also reported by Ayano and Mathunjwa [2]. From Figure 7(a) we note that the microrotation velocity increases in magnitude as heat generation increases near the surface, but decreases as heat absorption increases near

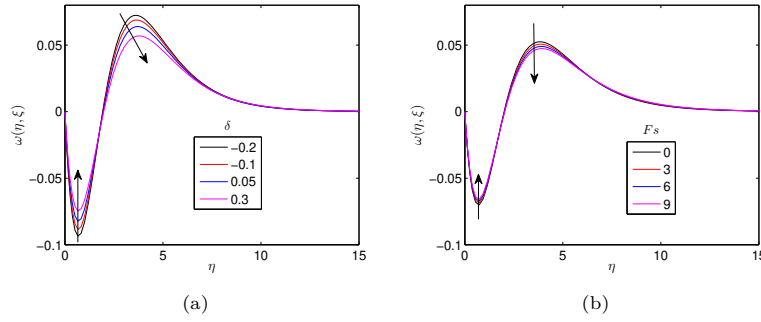


Figure 7. Effect of δ and F_s on microrotation

the surface. The opposite trend occurs away from the surface. Figure 7(b) depicts that the effect of the inertia coefficient is insignificant near the surface but the microrotation profiles increase slightly. Away from the boundary, the microrotation profiles decrease with the increase in the inertia coefficient.

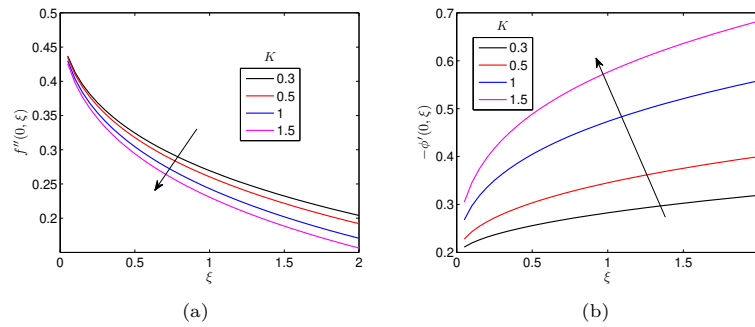


Figure 8. Effect of K on skin friction and Sherwood number

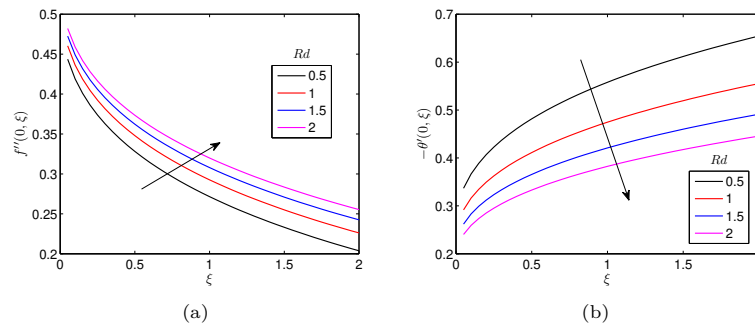


Figure 9. Effect of R_d on skin friction and Nusselt number

The variation of the local skin friction, wall couple stress, Nusselt number and Sherwood number with different parameters is depicted in Figures 8–11. Figure

8 presents the effect of the chemical reaction parameter on the local skin friction and the mass transfer coefficients. It is observed that higher values of the chemical reaction parameter lead to a reduction in the local skin friction coefficient. On the other hand, increasing chemical reaction enhances the rate of mass transfer. This is due to the fact that chemical reaction reduces the solutal boundary layer thickness and increases the mass transfer. An increase in the values of the chemical reaction implies more interaction of species concentration with the momentum boundary layer, thus having a more significant effect on the local Sherwood number. Figure 9 depicts the influence of the thermal radiation parameter on the local skin friction coefficient and the heat transfer rate. It is seen that the radiation flux reduces the heat transfer rate as the thermal radiation parameter increases. On the other hand, the local skin friction increases with increasing values of the thermal radiation parameter. Figure 10 shows the effect of Forchheimer quadratic drag number and coupling number on the skin friction coefficient. Increasing values of the Forchheimer and coupling number is observed to decrease the local skin friction.

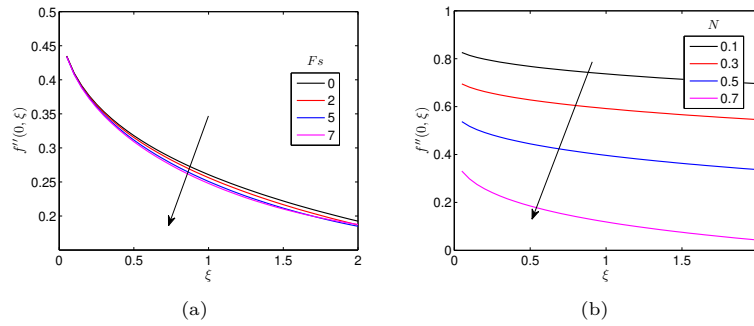


Figure 10. Effect of Fs and N on skin friction

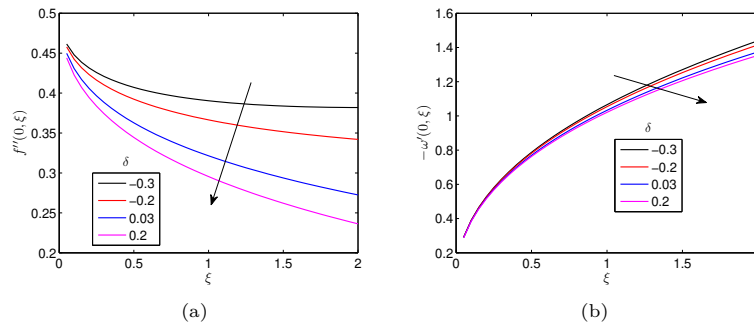


Figure 11. Effect of δ on skin friction and wall couple stress

Figure 11 documents the effect of the heat source/sink on the local skin friction and the wall couple stress coefficients. The local skin friction and the couple stress coefficient increase for smaller values of the heat source/sink parameter which implies that the heat source/sink has the tendency to increase the local skin friction and wall stress coefficient for $\delta < 0$. The influence of the heat source/sink parameter

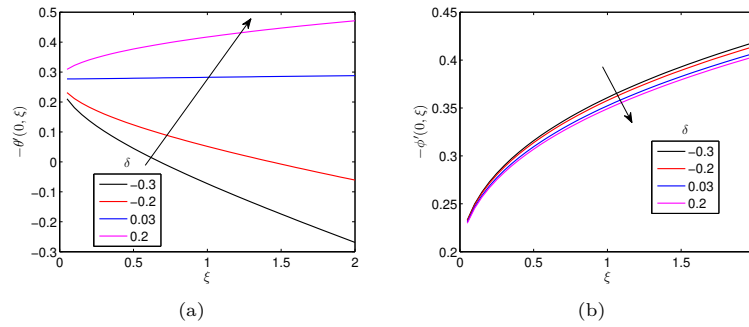


Figure 12. Effect of δ on Nusselt number and Sherwood number

on the local Nusselt number and Sherwood number is depicted in Figure 12. The figure indicates that the local Nusselt number increases for larger values of the heat source/sink and the local Sherwood number increases for small values of the heat source/sink. This means that the magnitude of the local Nusselt number increases for heat generation ($\delta > 0$) and the magnitude of the local Sherwood number increases for heat absorption ($\delta < 0$). Figures 13–14 illustrate the effect of the thermal radiation parameter, the coupling number, the chemical reaction parameter, and the Forchheimer number, on the wall couple stress coefficient. The wall couple stress increases with increasing values of the thermal radiation parameter and the coupling number, whereas the reverse trend is seen for the chemical reaction parameter and the Forchheimer parameter. We observe that the wall couple stress is weakly influenced by the thermal radiation and chemical reaction, but strongly influenced by the coupling number and Forchheimer number for increasing values of ξ . For increasing values of the coupling number, the effect of the microstructure becomes significant, hence the wall couple stress increases. With the inertial effects in a micropolar fluid saturated non-Darcy porous medium, the wall couple stress coefficient reduces. Figure 15 depicts the influence of the coupling number on the heat and mass transfer rates. It is observed from the figure that as the coupling number increases from 0 to 1, the rate of heat and mass transfer decreases. This is due to the presence of microscopic effects arising from the local structure and micromotion of the fluid elements.

The values of the local skin friction, heat and mass transfer coefficients are presented in Table 3 for different values n . For all the flow parameters, the local skin friction, heat and mass transfer coefficients are smaller in the turbulent boundary layer flows ($n = 1$) than in the concentrated particle flows ($n = 0$). This means that a strong concentration of microelements enhances the local skin friction as well as the rate of heat and mass transfer in the micropolar fluid flow. It is noted that the local skin friction, heat and mass transfer coefficients decrease with increasing values of the coupling and the Forchheimer number. The local skin friction and mass transfer coefficients are also observed to increase with increasing values of thermal radiation, while the reverse trend is true for the rate of heat transfer. The table also displays that the local skin friction and rate of mass transfer decrease with an increase in the values of the heat source/sink, while the reverse trend is observed on the rate of heat transfer. The local skin friction and the rate of heat transfer decrease with increasing values of the chemical reaction parameter and the

reverse trend are true for the rate of mass transfer. Finally, Table 4 shows that the local skin friction, heat, and mass transfer coefficients decrease with increasing values of the tangential coordinate ξ and increase with increasing values of the Hall parameter.

Table 3. Values of $f''(0, \xi)$, $-\theta'(0, \xi)$ and $-\phi'(0, \xi)$ for various values of N, K, Rd, δ, Fs, n when $\xi = 1$

N	Rd	δ	Fs	K	$n = 0$			$n = 1$		
					$f''(0, \xi)$	$-\theta'(0, \xi)$	$-\phi'(0, \xi)$	$f''(0, \xi)$	$-\theta'(0, \xi)$	$-\phi'(0, \xi)$
0.1	0.3	0.5	0.1	0.5	0.7415413	0.6243360	0.3587730	0.7352391	0.6240566	0.3585608
0.3	0.3	0.5	0.1	0.5	0.6247736	0.6208926	0.3562843	0.5876979	0.6191450	0.3549722
0.5	0.3	0.5	0.1	0.5	0.4912103	0.6167750	0.3531429	0.3882922	0.6118465	0.3493634
0.6	0.3	0.5	0.1	0.5	0.4167948	0.6143359	0.3511770	0.2604719	0.6068434	0.3452934
0.7	0.3	0.5	0.1	0.5	0.3361656	0.6115072	0.3487679	0.1058645	0.6005605	0.3398175
0.6	0.4	0.5	0.1	0.5	0.4218385	0.5879318	0.3516287	0.2662373	0.5807830	0.3458102
0.6	0.6	0.5	0.1	0.5	0.4307030	0.5441857	0.3524495	0.2763563	0.5376275	0.3467414
0.6	0.9	0.5	0.1	0.5	0.4417161	0.4940850	0.3535175	0.2889060	0.4882333	0.3479393
0.6	1.6	0.5	0.1	0.5	0.4607586	0.4169358	0.3554908	0.3105578	0.4122227	0.3501191
0.6	2	0.5	0.1	0.5	0.4690157	0.3866886	0.3563964	0.3199322	0.3824332	0.3511076
0.6	0.3	-0.2	0.1	0.5	0.5068426	0.0735351	0.3617850	0.3664429	0.0517940	0.3578390
0.6	0.3	-0.1	0.1	0.5	0.4886534	0.1784379	0.3595190	0.3356527	0.2096380	0.3540298
0.6	0.3	0	0.1	0.5	0.4726840	0.2710839	0.3575565	0.3265981	0.2559538	0.3529216
0.6	0.3	0.05	0.1	0.5	0.4654380	0.3135074	0.3566791	0.3180851	0.2996029	0.3518880
0.6	0.3	0.3	0.1	0.5	0.4352757	0.4954043	0.3531664	0.2824445	0.4858519	0.3477013
0.6	0.3	0.5	0.2	0.5	0.4165186	0.6142802	0.3511116	0.2602360	0.6067950	0.3452341
0.6	0.3	0.5	1.2	0.5	0.4138067	0.6137367	0.3504726	0.2579583	0.6063284	0.3446585
0.6	0.3	0.5	1.8	0.5	0.4122221	0.6134220	0.3501017	0.2566630	0.6060634	0.3443280
0.6	0.3	0.5	2.4	0.5	0.4106682	0.6131155	0.3497399	0.2554218	0.6058094	0.3440084
0.6	0.3	0.5	3	0.5	0.4091442	0.6128169	0.3493869	0.2542351	0.6055664	0.3436996
0.6	0.3	0.5	0.1	0.6	0.4134516	0.6139002	0.3791885	0.2564855	0.6063287	0.3737293
0.6	0.3	0.5	0.1	1.2	0.3977503	0.6120272	0.5206195	0.2377653	0.6041119	0.5167651
0.6	0.3	0.5	0.1	2	0.3838663	0.6106260	0.6669335	0.2212307	0.6024436	0.6640992
0.6	0.3	0.5	0.1	3	0.3722130	0.6096343	0.8145994	0.2073925	0.6012524	0.8124337
0.6	0.3	0.5	0.1	5	0.3576117	0.6086128	1.0499977	0.1901616	0.6000127	1.0484987

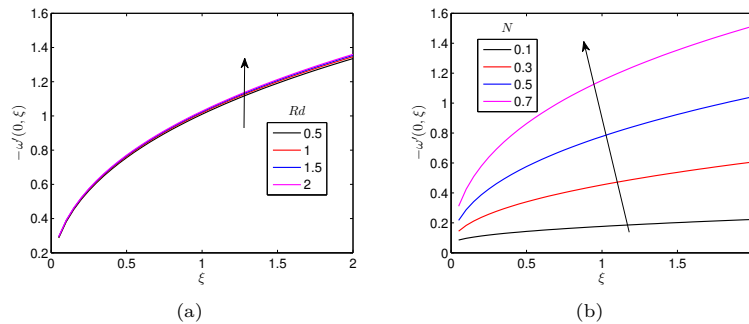


Figure 13. Effect of Rd and N on wall couple stress

5. Conclusion

This study analyzed two-dimensional MHD micropolar fluid flow, heat and mass transfer over a vertical plate embedded in a porous medium with heat source/sink,

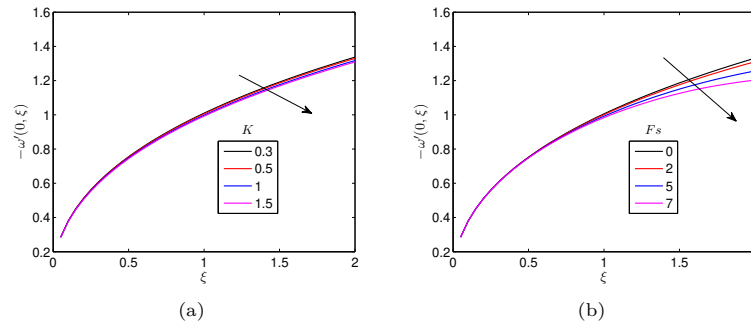


Figure 14. Effect of K and F_s on wall couple stress

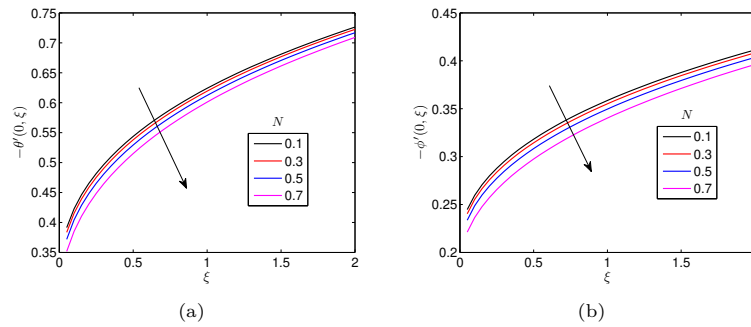


Figure 15. Effect of N on Nusselt Number and Sherwood number

Table 4. Values of $f''(0, \xi)$, $-\theta(0, \xi)$ and $-\phi'(0, \xi)$ for various values of ξ and β_h when $n = 1$

ξ	$\beta_h = 0.4$				$\beta_h = 1$				$\beta_h = 3$	
	$f''(0, \xi)$	$-\theta'(0, \xi)$	$-\phi'(0, \xi)$	$f''(0, \xi)$	$-\theta(0, \xi)$	$-\phi(0, \xi)$	$f''(0, \xi)$	$-\theta'(0, \xi)$	$-\phi(0, \xi)$	
0.2	0.3856138	0.4409326	0.2642840	0.3859158	0.4410107	0.2643638	0.3862507	0.4410973	0.2644522	
0.4	0.3434633	0.5004336	0.2927064	0.3438839	0.5005226	0.2928036	0.3443517	0.5006217	0.2929116	
0.6	0.3138024	0.5433735	0.3136991	0.3143088	0.5434664	0.3138055	0.3148729	0.5435700	0.3139240	
0.8	0.2903851	0.5779279	0.3308691	0.2909593	0.5780218	0.3309808	0.2916002	0.5781268	0.3311056	
1	0.2708507	0.6072247	0.3456110	0.2714806	0.6073181	0.3457258	0.2721849	0.6074229	0.3458542	
2	0.2028573	0.7132170	0.4002134	0.2036542	0.7132998	0.4003276	0.2045547	0.7133941	0.4004569	
3	0.1587063	0.7865516	0.4389674	0.1595474	0.7866185	0.4390702	0.1605123	0.7866967	0.4391885	
4	0.1261566	0.8440641	0.4697962	0.1269464	0.8441122	0.4698827	0.1278755	0.8441712	0.4699847	
5	0.1007451	0.8919864	0.4957218	0.1013945	0.8920128	0.4957885	0.1021957	0.8920498	0.4958706	
6	0.0803081	0.9333939	0.5182690	0.0807259	0.9333952	0.5183126	0.0813069	0.9334067	0.5183714	
7	0.0636351	0.9700533	0.5383292	0.0637228	0.9700251	0.5383460	0.0639861	0.9700073	0.5383779	
8	0.0499974	1.0030845	0.5564758	0.0496417	1.0030205	0.5564606	0.0494786	1.0029681	0.5564613	

chemical reaction, radiation and Hall effects. Also, the study presented the first opportunity to evaluate the accuracy and robustness of the OMD-BSLLM in finding numerical solutions of nonlinear coupled PDEs. The method was found to be convergent and gave accurate results after few iterations and using minimal grid points. The obtained results concurred with existing results in the literature for some limiting cases, hence validating the accuracy of the method. In the study, we found that the microrotation profiles change the sign from negative to positive within the boundary layer for all the flow parameters. The skin friction, heat and

mass transfer rates were found to be smaller in turbulent boundary layer flows than in concentrated particle flows. This implies that a strong concentration of microelements can enhance flow characteristics. The rest of the findings are summarized as follows:

- The higher values of the heat source/sink result in higher species concentration and heat transfer rate but produce lower fluid temperature, microrotation profiles, skin friction, couple stress coefficient, and mass transfer rate.
- An increase in the chemical reaction parameter enhances the local Sherwood number while reducing species concentration, microrotation profiles, skin friction, and couple stress coefficient.
- Thermal radiation tends to enhance micropolar fluid temperature, microrotation distribution, skin friction, and couple stress coefficient while reducing the rate of heat transfer.
- The presence of the inertial effects in micropolar fluid saturated non-Darcy porous medium reduces the microrotation component, skin friction, and couple stress coefficient.
- The higher values of the coupling number enhance the couple stress coefficient and reduce the skin friction, heat, and mass transfer rates.
- Increasing Hall parameter accelerates the local skin friction, Nusselt number and Sherwood number.

Acknowledgements

The authors are very grateful to the referee for the suggestions which helped to improve the writing of the paper.

References

- [1] M. S. Ayano, *Mixed convection flow of micropolar fluid over a vertical plate subject to Hall and Ion-slip currents*, Int. J. Eng. Appl. Sci., 2013, 5(3), 38–52.
- [2] M. S. Ayano and J. S. Mathunjwa, *Chemical reaction and radiation effects on unsteady MHD micropolar flow over a vertical plate with variable temperature*, Front. Heat Mass Transf., 2016, 7(9).
- [3] E. M. Aboeldahab and E. M. E. Elbarbary, *Hall current effect on magneto-hydrodynamic free-convection flow past a semi-infinite vertical plate with mass transfer*, Int. J. Engng. Sci., 2001, 39(14), 1641–1652.
- [4] F. Ahmad, *Effects of heat source/sink on MHD flow of micropolar fluids over a shrinking sheet with mass suction*, J. Basic. Appl. Sci. Res., 2014, 4(3), 2017–215.
- [5] T. Ariman, M. A. Turk and N. D. Sylvester, *Micro-continuum fluid mechanics A review*, Int. J. Engng. Sci., 1973, 11(8), 905.
- [6] T. Ariman, M. A. Turk and N. D. Sylvester, *Applications of micro-continuum fluid mechanics*, Int. J. Eng. Sci., 1974, 12(4), 273.
- [7] C. Canuto, M. Y. Hussaini, A. Quarteroni and T. Zang, *Spectral Methods in Fluid Dynamics*, Springer-Verlag, Berlin, 1988.

- [8] C. H. Chien and K. Chao, *Non-Darcian mixed convection along a vertical plate embedded in a porous medium*, Appl. Math. Model., 1990, 14, 482–488.
- [9] A. J. Chamkha, S. M. M. El-Kabeir and A. M. Rashid, *Coupled heat and mass transfer by MHD natural convection of micropolar fluid about a truncated cone in the presence of radiation and chemical reaction*, J. Nav. Archit. Mar. Eng., 2013, 10(2), 157–168.
- [10] A. J. Chamkha, *Coupled heat and mass transfer by natural convection about a truncated cone in the presence of magnetic field and radiation effects*, Numer. Heat Tr. A-Appl., 2001, 39(5), 511–530
- [11] A. J. Chamkha, S. M. M. EL-Kabeir and A. M. Rashad, *Heat and mass transfer by non-Darcian free convection from a vertical cylinder embedded in porous media with a temperature-dependent viscosity*, Int. J. Numer. Meth. Heat Fluid Flow, 2011, 21, 847–863.
- [12] A. J. Chamkha, S. M. M. EL-Kabeir and A. M. Rashad, *Unsteady coupled heat and mass transfer by mixed convection flow of a micropolar fluid near the stagnation point on a vertical surface in the presence of radiation and chemical reaction*, Prog. Comput. Fluid Dy., 2015, 15(3), 186–196.
- [13] A. C. Eringen, *Simple microfluids*, Int. J. Engng. Sci., 1964, 2, 205.
- [14] A. C. Eringen, *Microcontinuum Field Theories I: Foundations and Solids*, Springer-Verlag, New York, 1999.
- [15] A. C. Eringen, *Microcontinuum Field Theories-II: Fluent Media*, Springer, New York, 2001.
- [16] A. C. Eringen, *Theory of micropolar fluids*, J. Math. Mech., 1966, 16.
- [17] E. M. A. Elbashbeshy, T. G. Emam and E. A. Sayed, *Effect of thermal radiation on free convection flow and heat transfer over a truncated cone in presence of pressure work and heat source/sink*, Therm. Sci., 2016, 20(2), 555–565.
- [18] M. A. Hossain and K. Mohammad, *Effect of Hall current on hydromagnetic free convection flow near an accelerated porous plate*, Jpn. J. Appl. Phys., 1988, 27, 1531–1535.
- [19] M. A. Hossain and R. I. M. A. Rashid, *Hall effect on hydromagnetic free convection flow along a porous at plate with mass transfer*. J. Phys. Soc. Japan, 1987, 56, 97–104.
- [20] M. A. Hossain and H. S. Takhar, *Radiation effect on mixed convection along a vertical plate with uniform surface temperature*, Heat Mass Transf., 1996, 31, 243–248.
- [21] M. Kinyanjui, J. K. Kwanza and S. M. Uppal, *Magnetohydrodynamic free convection heat and mass transfer of a heat generating fluid past an impulsively started infinite vertical porous plate with Hall current and radiation absorption*, Energy Convers. Manag., 2001, 42, 917–931.
- [22] G. Lukaszewicz, *Micropolar fluids-Theory and Applications*, Birkhauser, Basel, 1999.
- [23] M. Modather, A. M. Rashad and A. J. Chamkha, *An analytical study of MHD heat and mass transfer oscillatory flow of a micropolar fluid over a vertical permeable plate in a porous medium*, Turkish J. Eng. Env. Sei., 2009, 33, 245–257.

- [24] S. R. Mishra, J. Mohanty and J. Das, *Free convective flow, heat and mass transfer in a micropolar fluid over a shrinking sheet in the presence of a heat source*, J. Eng. Phys. Thermophys., 2018, 91(4), 1043–1049.
- [25] V. M. Magagula, *On the multi-domain bivariate spectral local linearisation method for solving systems of nonsimilar boundary layer partial differential equations*, Int. J. Math. Math. Sci., 2019(2019), 1–18.
- [26] R. Muthucumaraswamy and G. S. Kumar, *Heat and mass transfer effects on moving vertical plate in the presence of thermal radiation*, Theoret. Appl. Mech., 2004, 31, 35–46.
- [27] I. Pop, *The effect of Hall current on hydromagnetic flow near accelerated plate*, J. Math. Phys. Sci., 1971, 5, 375–379.
- [28] P. Ranganathan and R. Viskanta, *Mixed convection boundary layer flow along a vertical porous medium*, Numer. Heat Transf., 1984, 7, 305–317.
- [29] A. Raptis and P. C. Ram, *Effects of Hall current and rotation*, Astrophys. Space Sci., 1984, 106(2), 257–264.
- [30] A. M. Rashad, Ali J. Chamkha and S. M. M. EL-Kabeir, *Effects of radiation and chemical reaction on heat and mass transfer by natural convection in a micropolar fluid-saturated porous medium with streamwise temperature and species concentration variations*, Heat Transf. Res., 2014, 45(8), 795–815.
- [31] A. M. Rashad, S. Abbasbandy and A. J. Chamkha, *Mixed convection flow of a micropolar fluid over a continuously moving vertical surface immersed in a thermally and solutally stratified medium with chemical reaction*, J. Taiwan Inst. Chem. Eng., 2014, 45(5), 2163–2169.
- [32] A. M. Rashad and S. M. M. EL-Kabeir, *Heat and mass transfer in transient flow by mixed convection boundary layer over a stretching sheet embedded in a porous medium with chemically reactive species*, J. Porous Media, 2010, 13(1), 75–85.
- [33] D. U. Srinivasacharya and U. Mendu, *Free convection in MHD micropolar fluid with radiation and chemical reaction effect*, Chem. Ind. Chem. Eng. Q., 2014, 20(2), 183–195.
- [34] L. N. Trefethen, *Spectral Methods in Matlab*, SIAM Philadelphia, 2000.
- [35] K. Vafai and C. L. Tien, *Boundary and inertia effects on flow and heat transfer in porous media*, Int. J. Heat Mass Transf., 1981, 24, 195–203.
- [36] K. A. Yih, *Effect of radiation on natural convection about a truncated cone*, Int. J. Heat Mass Transf., 1999, 42(23), 4299–4305.